cosity at constant temperature should depend to some extent on the relative abundances of OH^- and H_2O, this observation is consistent with a lack of pressure effects on water speciation up to superliquidus temperatures.

As determined from Fig. 3, the partial molar K_S of dissolved water is 18 ± 3 GPa, which is lower than the K_S values of geologically relevant silicate glasses, which range from 30 to 80 GPa (*7*). From obsidian to andesite and basalt compositions, for instance, K_S increases from 38 to 52 and 63 GPa, respectively, a trend that also correlates with the progressive disruption of the open network that is characteristic of silica-rich compositions. If our results for an andesite composition are representative of silicate glasses, the decreasing polymerization of the host silicate phase by water will enhance compressibility.

The partial molar volume of water in glasses (12 ± 0.5 cm^3/mol) is similar to 12.3 ± 0.3 cm^3/mol, which is the ambient volume of ice VII (*14*), the densest polymorph of ice near room temperature. We might expect structural differences between water dissolved in silicate glasses, as either OH^- or H_2O, and ice VII, which is made up of a three-dimensional open network of H_4O tetrahedra with a body-centered cubic oxygen sublattice. The K_S of dissolved water is also close to that of ice VII, namely, 23.9 ± 0.9 GPa (*14*). This high compressibility of ice VII stems from a shortening of the weaker hydrogen bonds. Even though the existence of OH^- and H_2O in glasses is well established, relatively little is known about their bonding to the host silicate phase. The fact that the compressibility of dissolved water is high and is independent of concentration suggests that a shortening of hydrogen bonds should also be a major compression mechanism for OH^- and H_2O. This shortening would also account for the decrease in shear modulus with water concentration (Fig. 4) and would point to a clustering of OH^-.

Similarities between the effects of water and alkali oxides have been revealed by viscosity (*15*) or electrical conductivity measurements (*16*). Water in glasses has a molar volume between those of Li_2O (9.3 cm^3/mol) and Na_2O (18.3 cm^3/mol) (*17*), but it is a component about two or three times more compressible than these alkali oxides (*18*). This property is additional evidence for compressible bonds between OH^- and H_2O and the silicate network, which are nonexistent for alkali oxides; it also agrees with the similarity in hydrogen bonding characteristics between OH^- and H_2O species in silicate glasses as revealed by NMR spectroscopy (*19*).

References and Notes

1. R. A. Lange, *Rev. Mineral.* **30**, 331 (1994).
2. B. Villemant, G. Boudon, J. C. Komorowski, *Earth Planet. Sci. Lett.* **140**, 259 (1996).
3. P. Richet *et al.*, *Chem. Geol.* **128**, 195 (1996).
4. J. R. Sandercock, in *Light Scattering in Solids III*, M. Cardona and G. Güntherodt, Eds. (Springer-Verlag, Berlin, 1982), pp. 173–206.
5. G. Tammann and E. Jenckel, *Z. Anorg. Allg. Chem.* **184**, 416 (1929).
6. P. Richet *et al.*, *Eos (Fall Suppl.)* **77**, 799 (1996).
7. J. D. Bass, in *Handbook of Physical Constants*, T. J. Ahrens, Ed. (American Geophysical Union, Washington, DC, 1995), vol. 2, pp. 45–63.
8. P. Richet and Y. Bottinga, *Geochim. Cosmochim. Acta* **44**, 1535 (1980).
9. E. Stolper, *Contrib. Mineral. Petrol.* **81**, 1 (1982).
10. L. A. Silver *et al.*, *ibid.* **104**, 142 (1990).
11. H. Keppler and N. S. Bagdassarov, *Am. Mineral.* **78**, 1324 (1993); M. Nowak and H. Behrens, *Geochim. Cosmochim. Acta* **59**, 3445 (1995).
12. G. Adam and J. H. Gibbs, *J. Chem. Phys.* **43**, 139 (1965).
13. P. Richet and Y. Bottinga, *Rev. Mineral.* **32**, 67 (1995).
14. R. J. Hemley *et al.*, *Nature* **330**, 737 (1987).
15. D. B. Dingwell, C. Romano, K. U. Hess, *Contrib. Mineral. Petrol.* **124**, 19 (1996).
16. M. Takata *et al.*, *J. Am. Ceram. Soc.* **64**, 719 (1981).
17. H. Doweidar, *J. Non-Cryst. Solids* **194**, 155 (1996).
18. J. Schroeder, thesis, Catholic University of America, Washington, DC (1974).
19. H. Eckert *et al.*, *J. Phys. Chem.* **92**, 2055 (1988).

20. We thank A. M. Lejeune for the loan of the samples, G. Boudon and B. Villemant for analyses, and anonymous reviewers for helpful comments. The work was supported by the European Union Training and Mobility of Researchers grant "hydrous melts."

20 March 1998; accepted 4 June 1998

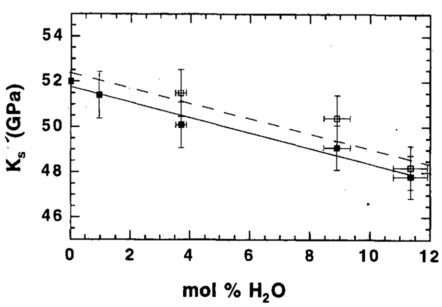

Fig. 3. K_S values of compacted (open squares) and relaxed (solid squares) hydrous andesite glasses. The solid line is a linear fit to the data for the relaxed samples, and the dashed line shows the values that are determined from this fit for the compacted glasses by assuming a value of 4 for K'_0, which is the 1-bar derivative of K_S, and a mean pressure of vitrification of 1.5 kbar.

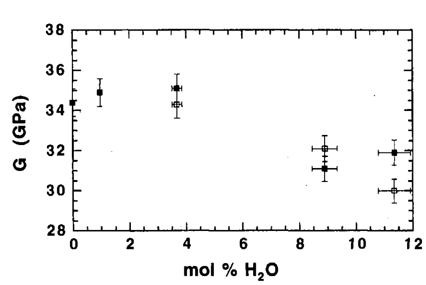

Fig. 4. *G* values of compacted (open squares) and relaxed (solid squares) hydrous andesite glasses.

Evidence for Large Earthquakes in Metropolitan Los Angeles

Charles M. Rubin,* Scott C. Lindvall, Thomas K. Rockwell

The Sierra Madre fault, along the southern flank of the San Gabriel Mountains in the Los Angeles region, has failed in magnitude 7.2 to 7.6 events at least twice in the past 15,000 years. Restoration of slip on the fault indicated a minimum of about 4.0 meters of slip from the most recent earthquake and suggests a total cumulative slip of about 10.5 meters for the past two prehistoric earthquakes. Large surface displacements and strong ground motions resulting from greater than magnitude 7 earthquakes within the Los Angeles region are not yet considered in most seismic hazard and risk assessments.

The potential for damage from earthquakes along reverse faults in the Los Angeles region has been illustrated by the 1971 San Fernando, 1987 Whittier Narrows, 1991 Sierra Madre, and 1994 Northridge earthquakes (*1*–*3*). These earthquakes have sparked questions regarding the maximum magnitude of earthquakes on reverse faults in the greater Los Angeles region (*4*–*8*) and, in particular, the central Transverse Ranges (*3*, *9*–*14*). Although large events on reverse faults could affect millions of people, most earthquake hazard assessments in southern California have traditionally focused on the San Andreas fault and adjacent strike-slip faults (*15*, *16*). Geodetic studies indicate that the Los Angeles basin from the Jet Propulsion Laboratory to the Palos Verdes Peninsula is shortening by 5 (*10*) to 7.9 mm $year^{-1}$ (*12*), partly along reverse faults. One problem in making an assessment has been that paleoseismic data on these reverse faults are sparse. Here, we present paleoseismic data from the Sierra Madre fault, one of the major reverse faults in

C. M. Rubin, Department of Geology, Central Washington University, Ellensburg, WA 98926, USA. S. C. Lindvall, William Lettis and Associates, 27201 Tourney Road, Suite 201-B, Valencia, CA 91355, USA. T. K. Rockwell, Department of Geological Sciences, San Diego State University, San Diego, CA 92182, USA.

*To whom correspondence should be addressed

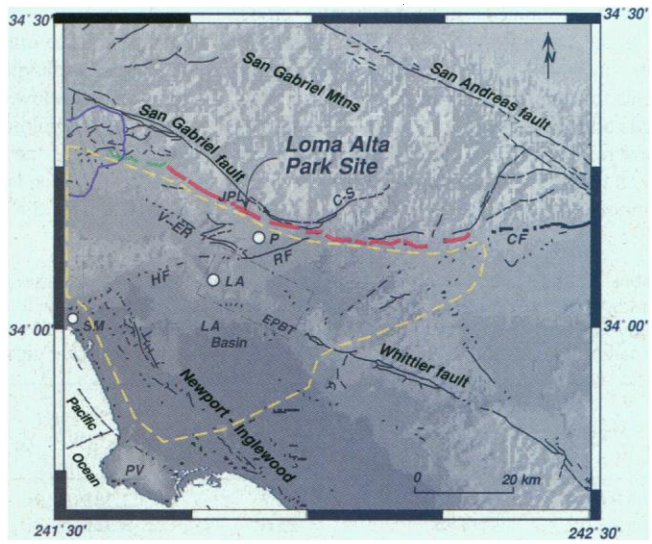

Fig. 1. Map of southern California showing major faults. CF, Cucamonga fault; C-S, Clamshell-Sawspit fault; EPBT, Elysian Park blind thrust; JPL, Jet Propulsion Laboratory; LA, Los Angeles; HF, Hollywood fault; P, Pasadena; PV, Palos Verdes; RF, Raymond fault; SM, Santa Monica; V-ER, Verdugo–Eagle Rock fault. The Sierra Madre fault is shown as heavy red lines; the 1971 San Fernando earthquake surface rupture is shown as heavy green lines. The Northridge aftershock zone is shown as blue hatched lines. Yellow dashes surround the dense metropolitan population of the Los Angeles, San Gabriel, and San Fernando basins.

the Los Angeles region (Fig. 1). The paleoseismic site is located ~18 km north of downtown Los Angeles (Fig. 2) and contains evidence of two large prehistoric earthquakes in the past 15,000 years.

The Sierra Madre–Cucamonga fault system bounds the southern flank of the central San Gabriel Mountains and extends for about 95 km along the northern edge of the densely populated San Fernando and San Gabriel valleys (Fig. 1) (*13*, *17*). The northwestern 19-km section of the Sierra Madre fault (the San Fernando fault) ruptured during the 1971 moment magnitude (M_w) = 6.7 San Fernando earthquake (Fig. 1), caused \$558 million in damage, and claimed 64 lives (*1*, *18*). On the basis of regional geologic mapping, geomorphic expression of the fault, and some paleoseismic studies, Crook *et al.* (*17*) concluded that no major earthquakes had occurred east of the 1971 rupture on this fault for at least the past several thousand years and possibly for the past 11,000 years. They also argued that the central section of the Sierra Madre fault has a lower slip rate than other sections, such as the Cucamonga fault to the east and the San Fernando fault to the west. Yet some of the high peaks of the San Gabriel Mountains are located along the central section.

We studied the fault where it crosses an uplifted terrace that lies east of Millard Canyon in Loma Alta Park (Fig. 2). Geomorphic evidence of prehistoric deformation along the Sierra Madre fault here consists of a >2-m scarp that cuts a late Quaternary stream terrace. We excavated a trench across the well-expressed scarp immediately north of the parking lot of Loma Alta Park (Fig. 2). This uplifted terrace no longer receives active deposition and lies between the deeply incised Millard Canyon on the west and West Ravine on the east (Fig. 2).

The oldest exposed stratigraphic unit is a crudely stratified and locally imbricated, boulder- to pebble-sized gravel with a coarse sand matrix (Fig. 3, unit 1) (*19*). Overlying the coarse gravel is a fine sandy gravelly loam (Fig. 3, unit 2) (*19*). A buried soil (A, B_t, and C horizon), with a 50-cm-thick B_t horizon, is developed within the fine-grained alluvium of unit 2 and the uppermost coarse gravel of stratigraphic unit 1. Detrital charcoal in the buried A horizon of this unit yielded ^{14}C ages of about 16 and 24 thousand years ago (ka) (Table 1). Overlying the fine-grained alluvial unit is a wedge-shaped deposit of massive, pebbly, coarse- to fine-grained sand (Fig. 3, unit 3) (*19*). The two alluvial units (units 1 and 2), the buried soil, and colluvium (unit 3) are exposed in the footwall beneath a gently north dipping fault. Only the coarse alluvium (unit 1) is present in the hanging wall. A massive unfaulted unit of boulders and gravel in an organic-rich silt and sand matrix (Fig. 3, unit 4a) (*19*) overlies the fine-grained alluvium and colluvial wedge. This gravel unit thins southward and laterally grades into extensively bioturbated, organic-rich silty sand (Fig. 3, unit 4b) (*19*).

Radiocarbon ages on detrital charcoal indicate that units 2 through 4a are late to latest Pleistocene in age and that unit 4b is younger (Table 1) (*20*). Four fragments of detrital charcoal from unit 3 yielded ages between 18,500 ± 1000 years before present (yr B.P.) and 34,300 ± 800 ^{14}C yr. B.P. (Table 1); we interpret the youngest age of 18.5 ka as a maximum age for deposition of the colluvial deposits. Four fragments of detrital charcoal from unit 4a yielded ages of 10,600 ± 1000 to 18,200 ± 1000 yr B.P. (Table 1); thus, the maximum age of the colluvium is about 10,600 ± 1000 yr B.P. (Table 1). We interpret the wide range of detrital radiocarbon ages as the result of recycling detrital charcoal from older alluvial deposits exposed uphill and north of the fault scarp (*21*). Age constraints on colluvial unit 4b are less certain than those for older stratigraphic units because of extensive bioturbation that typically occurs in A horizons (topsoil). Two detrital charcoal fragments re-

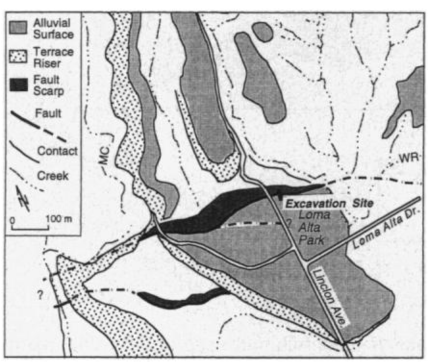

Fig. 2. Map of the Loma Alta Park paleoseismic site showing location of trench, fault zones, and scarp. The Sierra Madre fault shown as heavy black lines, dashed where inferred. MC, Millard Canyon; WR, West Ravine.

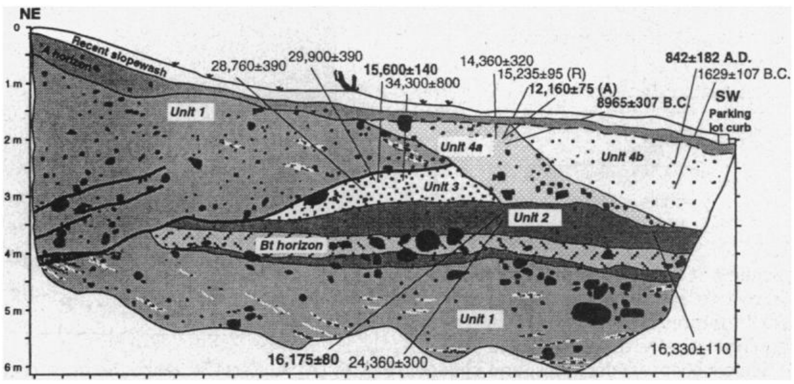

Fig. 3. Cross section through sediments in trench wall showing fault traces, stratigraphic units, and radiocarbon dates. A, angular detrital charcoal fragment; R, rounded detrital charcoal fragment. Faults are shown as heavy lines. Scale is shown in meters, with no vertical exaggeration. Radiocarbon ages are quoted in ^{14}C years before present, except calendric ages quoted as ka (years B.P.).

covered from a bulk sample yielded radiocarbon ages of 1107 ± 170 and 3350 ± 80 yr B.P. (Table 1). We interpret these young radiocarbon ages as minimum ages because it is likely that the charcoal was incorporated biogenically after deposition of unit 4b.

The Sierra Madre fault appears in the trench wall as a single trace (with minor faults) in a zone about 0.5 m wide within the hanging wall of coarse alluvial gravels (Fig. 3). Several lines of evidence were used to identify prehistoric earthquakes. Truncation of stratigraphic units is the clearest evidence for past events. We also interpret wedge-shaped colluvial deposits to represent material shed off the fault scarp immediately after surface-rupturing earthquakes. As a reverse fault ruptures the surface, the hanging wall block overrides the footwall block. The oversteepened slope on the hanging wall quickly collapses, forming a colluvial wedge that overlies the footwall and surface rupture of the fault (Fig. 4).

Trench wall exposures show two colluvial wedges (Fig. 3, units 3 and 4a). The upper colluvial wedge contains southward thinning coarse gravels (unit 4a), lies directly above the fault zone, and is the primary evidence for the most recent earthquake. The wedge-shaped geometry and composition of the unit imply that it is a colluvial deposit derived from unit 1, exposed on the fault scarp shortly after an earthquake. Rapid denudation of the oversteepened slope on the hanging wall formed this colluvial wedge (Fig. 4). Units 2 and 3 and the buried soil have been faulted and subsequently eroded from the hanging wall block. Restoration of the dip slip component of motion on the fault reveals the approximate geometry of the alluvial and colluvial deposits and buried soil before the most recent earthquake and gives a minimum of ~3.8 to 4.0 m of dip slip from the most recent earthquake (Fig. 5A).

The presence of an older colluvial wedge (unit 3) and the truncation of the subhorizontal fine-grained alluvium (unit 2) and the buried soil horizon below the fault zone indicate that there was a penultimate earthquake on the fault. Restoration of the upper plate to below the buried soil yielded a cumulative minimum slip of ~10.5 m for the last two events (Fig. 5B). In

Table 1. Radiocarbon analyses of charcoal samples. Samples are listed in stratigraphic order. The stratigraphic unit indicates the stratum collected; see Fig. 3 for sample location. Reported ^{14}C ages use Libby's half-life (5568 years); sample and standard ^{13}C values are normalized to −25 per mil where shown in parentheses. Analytical uncertainties are 1 SD and reflect the total uncertainty in the measurement.

Sample	Strati-graphic unit	$\delta^{13}C$ (per mil)	^{14}C age (years B.P. ± 1σ)	Calendar age range* (years B.P. ± 2σ)
LAP-MRT-1	4b	−25.7	1,185 ± 95	937– 1,277
LAP-MRT-2	4b	−25.6	3,335 ± 35	3,471– 3,630
LAP-MRT-3	4a	−25.3	9,495 ± 75	10,349–10,902
LAP-BS-1†	4a	−23.3	12,160 ± 75	13,897–14,530
LAP-14	4a	−23.3	14,360 ± 320	16,445–17,924
LAP-BS-2†	4a	−23.7	15,235 ± 95	17,901–18,405
LAP-4	3	−23.3	15,600 ± 140	18,191–18,816
LAP-5	3	−23.8	28,760 ± 370	NA
LAP-12	3	−25.1	29,550 ± 710	NA
LAP-9	3	−25.0	29,900 ± 390	NA
LAP-MRT-5	3	(−25.0)	34,300 ± 800	NA
LAP-MRT-4	2	−23.4	16,175 ± 80	18,804–19,349
LAP-10	2	−22.0	16,330 ± 110	18,912–19,604
LAP-13	2	−23.4	24,360 ± 300	NA

*Dendrochronologically calibrated calendar ages were calculated with the University of Washington Calibration Program (23). †Sample LAP-BS-1 is composed of angular detrital fragments; LAP-BS-2 is composed of rounded detrital fragments.

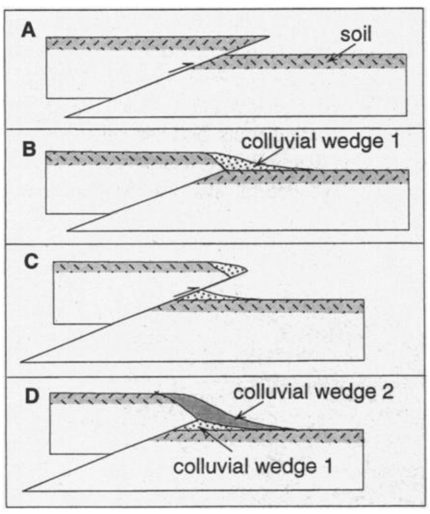

Fig. 4. Schematic development of colluvial wedges from two successive earthquakes. (**A**) Earthquake 1 ruptures the ground surface; scarp is known schematically as an unstable overhang. (**B**) Scarp collapses, degrades, and sheds debris, forming colluvial wedge 1. (**C**) Earthquake 2 ruptures ground surface and offsets colluvial wedge 1. (**D**) Scarp collapses, degrades, and sheds debris to form colluvial wedge 2. Surficial soil and colluvial wedge 1 are no longer preserved in the upper plate.

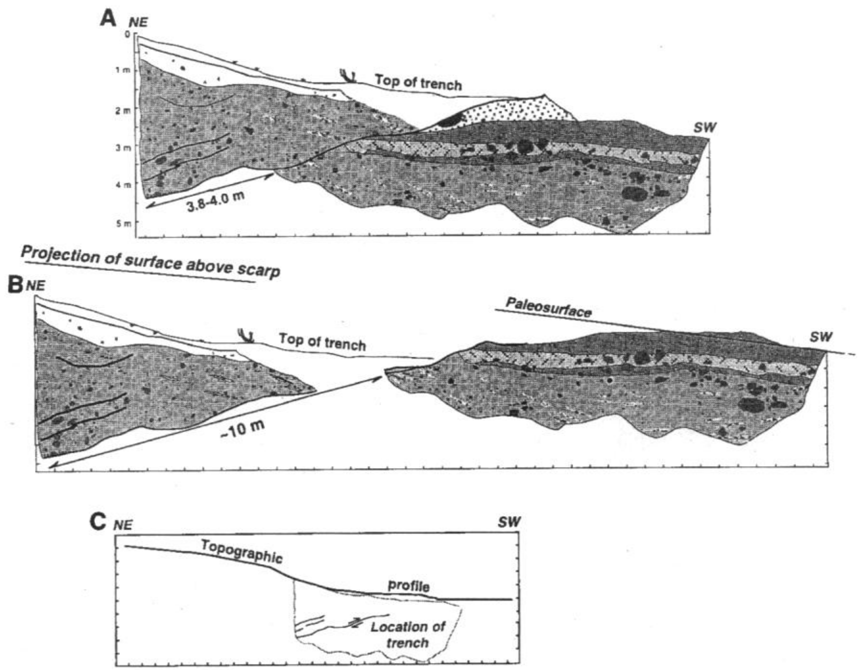

Fig. 5. (**A**) Restoration from the most recent earthquake yields a minimum slip of 3.8 to 4.0 m. In this restoration, the tip of the upper plate is restored to below the lower colluvial wedge; the restoration does not account for any slip on secondary faults within the hanging wall. (**B**) Restoration of slip from the last two earthquakes showing a minimum of ~10 m. Here, the upper plate is restored to below the B_t horizon, and the buried paleosurface surface is matched to the topographic profile of the fault scarp. (**C**) Detailed topographic profile of fault scarp surveyed with an electronic distance meter/theodolite.

this restoration, we assumed that the buried soil and fine-grained alluvium were continuous across the hanging wall. This restoration also yielded a smooth initial paleosurface between the upper surface of the scarp and the paleosurface exposed in the trench exposure (Fig. 5, B and C).

The youngest radiocarbon dates on small fragments of charcoal from the upper colluvial wedge (unit 4b) are about 10,000 ka. Therefore, the most recent surface-rupturing earthquake at Loma Alta Park occurred within the past 10,000 years. A soil development index (SDI) age of ~10 ka for the buried soil is consistent with this age of faulting (*22*). Because the buried soil was stripped from the hanging wall, both earthquakes must have postdated the formation of the soil. This observation suggests that the surface was stable for some time before faulting.

No clear evidence exists for the elapsed time between events. However, the steepness of the southern slope of unit 3 (40°) indicates that it was buried by younger material before much degradation occurred, suggesting that the most recent earthquake followed shortly after the penultimate event. Observations of historical scarps suggest that gravitational collapse may occur within a few decades of an earthquake (*23*). There is no evidence for additional slip events in the trench, although the possibility of missing events on unrecognized fault strands beyond reach of the trench cannot be ruled out.

The paleoseismic data imply that the average slip rate for the Sierra Madre fault at this site is about 10.5 m over the past 18 ka, or 0.6 mm^{-1} year. Although there is debate on the maximum size of earthquakes in the greater Los Angeles region, our data suggest that prehistoric earthquakes at the Loma Alta site are substantially larger than other historically observed earthquakes along reverse faults in the Los Angeles region (*24*). Large displacements of 4 m or greater are inconsistent with short (15 to 20 km) ruptures involving only single segments of the Sierra Madre fault and imply that past earthquakes at this location ruptured larger dimensions of the fault zone. In comparison, the 1971 $M_w = 6.7$ San Fernando earthquake that ruptured the northwestern 19 km of the Sierra Madre fault zone produced a maximum surface reverse displacement of ~2 m (*1–3*).

On the basis of the slip in the most recent earthquake at the Loma Alta site, we can infer the size of the prehistoric earthquakes. Two approaches are used to estimate maximum magnitude. One approach uses a regression relating either maximum surface displacement or average surface displacement to moment magnitude M_w (*25*). Using 5.25 m (10.5-m total slip divided by two events) as the maximum displacement yields a $M_w = 7.2 \pm 0.4$. If we assume that 5.25 m represents the average surface displacement, the regression predicts a $M_w = 7.5 \pm 0.5$. Another approach uses seismic moment (*26*). Assuming an average slip of 3.8 m (minimum slip measured in the trench), a strike length of 65 km, and a seismogenic depth of 18 km yields a seismic moment of 1.92×10^{27} dyne·cm for the most recent earthquake (*27*). With an average slip of 5.25 m, a strike length of 65 km, and a seismogenic depth of 18 km, the seismic moment for the most recent earthquake is 2.65×10^{27} dyne·cm (*27*). Converting seismic moment to moment magnitude from the previous two estimates (*28*) yields $M_w \approx 7.5$ to 7.6 for the most recent earthquake.

The penultimate earthquake was similar in size to the most recent earthquake. Our paleoseismic data thus imply that the past two earthquakes were greater than $M_w = 7$, which is substantially larger than historical earthquakes along other reverse faults in the greater Los Angeles region (*24*).

Although elsewhere in the Transverse Ranges, $M > 7$ earthquakes occurred in 1812, 1927, and 1952 (*29*), here we have direct evidence that large earthquakes have occurred close to Los Angeles. Our results support Hough's model (*30*) that most of the seismic moment release in the greater Los Angeles area is by infrequent but large events ($M_w = 7.4$ to 7.5). Damage from large magnitude earthquakes along the Sierra Madre fault would be substantially different from that produced in the 1994 $M_w = 6.7$ Northridge earthquake, with near field, high-amplitude ground motions over a much larger area and for a longer duration (*31*). Unlike the Northridge earthquake that ruptured northward away from the metropolitan region, a magnitude 7 or greater earthquake on the Sierra Madre fault would rupture southward, directing energy into the densely populated basin. Large surface displacements, as well as strong ground motions, have the potential for disrupting lifeline systems and producing substantial damage to modern buildings. In the greater Los Angeles region, such ground motions are not yet considered in estimates of seismic hazard.

References and Notes

1. B. Kamb *et al.*, *U.S. Geol. Surv. Prof. Pap.* **733**, 41 (1971).
2. E. Hauksson and J. Jones, *J. Geophys. Res.* **94**, 9569 (1989); E. Hauksson, *Bull. Seismol. Soc. Am.* **84**, 1058 (1991).
3. E. Hauksson, L. M. Jones, K. Hutton, *J. Geophys. Res.* **100**, 12335 (1995).
4. J. F. Dolan *et al.*, *Science* **267**, 199 (1995).
5. S. E. Hough, *ibid.*, p. 211.
6. Southern California Earthquake Center, *Bull. Seismol. Soc. Am.* **85**, 379 (1995).
7. D. Jackson, *Seismol. Res. Lett.* **67**, 3 (1996).
8. Dolan *et al.* (*4*) concluded that the historical seismicity has not kept pace with the rate of tectonic convergence across the greater Los Angeles region. They suggested that an earthquake between magnitude 7.2 and 7.5 would be necessary to relieve the excess strain.
9. T. Davis *et al.*, *J. Geophys. Res.* **94**, 9644 (1989).
10. K. Fleigel *et al.*, *ibid.* **98**, 21677 (1993).
11. E. Gath *et al.*, *Geol. Soc. Am. Abstr. Programs Cordilleran Sect.* **24**, 26 (1992); E. Hauksson and L. Jones, *J. Geophys. Res.* **96**, 8143 (1991).
12. K. Hudnut *et al.*, *Seismol. Res. Lett.* **65**, 59 (abstr.) (1994).
13. D. Morton and J. Matti, *U.S. Geol. Surv. Prof. Pap.* **1339**, 179 (1987).
14. T. Rockwell *et al.*, *Geol. Soc. Am. Abstr. Programs* **20**, 224 (1988); J. Shaw, thesis, Princeton University, Princeton, NJ (1993); J. Shaw and J. Suppe, *Geol. Soc. Am. Bull.* **106**, 607 (1994); *J. Geophys. Res.* **101**, 8623 (1996).
15. J. Davis *et al.*, *Calif. Div. Mines Geol. Spec. Publ. 60* (1982); Working Group on California Earthquake Probabilities, *U.S. Geol. Surv. Open-File Rep. 88-398* (1988); T. Toppozada *et al.*, *Calif. Div. Mines Geol. Spec. Publ. 102* (1993).
16. S. Wesnousky, *J. Geophys. Res.* **91**, 12587 (1986).
17. R. Crook *et al.*, *U.S. Geol. Surv. Prof. Pap.* **1339**, 27 (1987).
18. R. Kachadoorian, *ibid.*, p. 5.
19. Unit 1 is yellow to pale brown, unconsolidated fine- to very coarse–grained sand and gravel, containing abundant cobbles, boulders, and moderately weathered diorite clasts and local cross-bedded sand and imbricated cobbles. Unit 2 is tan to yellowish-brown, sandy, gravelly loam. Unit 3 is massive, yellowish-brown, coarse- to fine-grained sand, with abundant pebbles and cobbles. Unit 4a is massive, light brown, unconsolidated organic silt and coarse- to fine-grained sand, containing abundant cobbles and pebbles. Unit 4b is brown, extensively bioturbated, unconsolidated medium to very fine organic-rich sand and silt, containing sparse gravel. A buried soil exposed on the footwall includes a weak to moderately developed 46-cm-thick B_t horizon, 10YR5/4 moist color soil and a 38-cm-thick A_b horizon, 10YR5/3 moist color soil in units 1 and 2, and a 0- to 14-cm-thick colluvial A horizon with 10YR5/3 moist color soil in unit 3.
20. Radiocarbon dating was performed by G. Burr at the University of Arizona. Dendrochronogically calibrated calendar ages were calculated with (*32*) method B, a 20-year calibration curve, and 2σ uncertainty. Radiocarbon ages are not the same as calendric ages; radiocarbon ages are corrected for the reservoir effect [M. Stuiver and H. A. Pollach, *Radiocarbon* **3**, 355 (1977)]. For samples less than 8000 ^{14}C years old, the calibration relied on radiocarbon dates from tree rings of known ages. For charcoal ages greater than 13 ka, we used Stuiver and Reimer's (*32*) calibration method; errors were rounded to the nearest 1 ka. Recent comparisons of radiocarbon and U/Th ages on corals have, however, shown that radiocarbon ages in the range of about 10,000 years to 14,000 years correspond to calendric ages about 3000 years older [R. L. Edwards, J. W. Beck, G. S. Burr, D. J. Donahue, J. M. A. Chappell, *Science* **260**, 962 (1993)].
21. Detrital charcoal provides a maximum age estimate of the strata that contain it. Three lines of evidence support the presence of older reworked charcoal in younger stratigraphic units: (i) A radiocarbon age of 29 ± 4 ^{14}C years B.P. was obtained from an older surface located about 1 km uphill from the excavation site. Detrital charcoal from these older alluvial units is incorporated into the younger alluvial units, which are exposed in our excavation. (ii) Angular and rounded charcoal fragments were analyzed from the same sample locality. The angular fragment yielded a radiocarbon age of 14.2 ± 1000 years B.P., and the rounded fragment yielded an older radiocarbon age of 18.2 ± 1000 years B.P. (iii) Radiocarbon ages vary by a factor of 2 in the same stratigraphic horizon, which suggests recycling of older detrital charcoal. The buried colluvial wedges (units 3 and 4a) are well stratified and show little evidence of bioturbation; thus, incorporation of young carbon is unlikely in these well-stratified deposits. However, in extensively bioturbated deposits, such as unit 4b, it is likely that young carbon ages reflect incorporation of young carbon.

22. SDI is generated by assessing the relative difference between the present development of the soil and that of its parent material [J. Harden, *Geoderma* **28**, 1 (1982)]. For the buried soil exposed in the trench, the parent material is gravelly sand with sparse primary clay. Because SDI values are, in part, thickness-dependent [T. Rockwell, C. Loughman, P. Merifield, *J. Geophys. Res.* **95**, 8593 (1990)], all SDIs were normalized to 250 cm, which was the thickness of the C horizon in the trench. Two trench profiles yielded SDI values of ~ 20, which correspond to an age estimate of 10.5 +22/−7 ka (2σ error).
23. M. Clark, *U.S. Geol. Surv. Prof. Pap.* **787**, 190 (1972).
24. For example, the 1971 M_w 6.7 San Fernando, 1987 M_w 5.9 Whittier Narrows, 1991 M_w 5.8 Sierra Madre, and 1994 M_w 6.7 Northridge earthquakes.
25. D. Wells and K. Coppersmith, *Bull. Seismol. Soc. Am.* **84**, 974 (1994).
26. The size of an earthquake is best represented by the seismic moment M_o. The seismic moment is the product of the fault surface area, the average displacement on the fault, and the rigidity of the rock.
27. On the basis of previous fault segmentation models (*16, 17*), we used a 65-km rupture length that represents multiple short segments, from Big Tujunga to San Antonio Canyon. A rupture length of 65 km corresponds to the portion of the fault between the 1971 San Fernando rupture and the Cucamonga fault. By varying the depth or strike length by 20%, the magnitude will only change by 0.05 unit. Large surface displacements suggest that the Sierra Madre fault breaks across multiple, relatively short segments [as defined by (*17*)], unlike the 1971 event that ruptured a single segment. The historical earthquake rupture patterns of large-magnitude earthquakes on intracontinental reverse faults show that multiple ruptures across segment boundaries are common [C. Rubin, *Geology* **24**, 989 (1996)].
28. With the equation $M_w = [2/3 \log (M_o) - 16]$ of T. Hanks and T. Kanamori [*J. Geophys. Res.* **84**, 2348 (1979)]. We used 3.00×10^{11} dyne·cm for the shear modulus in the seismic moment calculations.
29. T. Hanks [*Bull. Seismol. Soc. Am.* **69**, 451 (1979)] for the $M = 7.3$ Lompoc, California, earthquake and C. Richter [*Elementary Seismology* (Freeman, New York, 1958)] for the 1812 Santa Barbara Channel earthquake.
30. Hough's (*5*) model assumes the distribution of earthquakes in the Los Angeles region will follow a fractal distribution of rupture areas. This model predicts that about one M_w = 7.4 to 7.5 earthquake should occur every 245 to 325 years and about six M_w = 6.6 earthquakes within this same time span.
31. T. H. Heaton, J. F. Hall, D. J. Wald, M. W. Halling, *Science* **267**, 206 (1995); C. Saikia, *Bull. Seismol. Soc. Am.* **83**, 760 (1993); *ibid.*, p. 379.
32. M. Stuiver and P. Reimer, *Radiocarbon* **35**, 214 (1983).

33. We thank K. Sieh for helpful discussions, C. Walls for assistance in the field, and the County of Los Angeles for providing access to Loma Alta Park. This research was supported by the Southern California Earthquake Center (SCEC). SCEC is funded by NSF cooperative agreement EAR-8920136 and U.S. Geological Survey cooperative agreements 14-08-0001-A0899 and 1434-HQ-97AG01718. This is SCEC contribution 442.

17 March 1998; accepted 14 May 1998

Molecular Coproscopy: Dung and Diet of the Extinct Ground Sloth *Nothrotheriops shastensis*

Hendrik N. Poinar, Michael Hofreiter, W. Geoffrey Spaulding, Paul S. Martin, B. Artur Stankiewicz,* Helen Bland, Richard P. Evershed, Göran Possnert, Svante Pääbo

DNA from excrements can be amplified by means of the polymerase chain reaction. However, this has not been possible with ancient feces. Cross-links between reducing sugars and amino groups were shown to exist in a Pleistocene coprolite from Gypsum Cave, Nevada. A chemical agent, *N*-phenacylthiazolium bromide, that cleaves such cross-links made it possible to amplify DNA sequences. Analyses of these DNA sequences showed that the coprolite is derived from an extinct sloth, presumably the Shasta ground sloth *Nothrotheriops shastensis*. Plant DNA sequences from seven groups of plants were identified in the coprolite. The plant assemblage that formed part of the sloth's diet exists today at elevations about 800 meters higher than the cave.

The polymerase chain reaction (PCR) has opened up new possibilities in ecology, archaeology, and paleontology by making it possible to retrieve DNA sequences from several previously untapped sources (*1*). One such source is feces, from which amplified DNA sequences allow identification of the species or individual from which the droppings originated as well as aspects of the diet and parasitic load of the animal (*2*). Large amounts of ancient feces (coprolites) can be found in certain dry caves or rock shelters—for example, in the southwestern United States (*3*). To investigate whether it may be possible to amplify DNA from such material, we have analyzed coprolites from Gypsum Cave about 30 km. east of Las Vegas, Nevada. These have been attributed to the Shasta ground sloth, *Nothrotheriops shastensis* (*4*), which became extinct about 11,000 years ago (*5*). Initial experiments showed that extraction protocols developed for contemporary fecal material did not yield amplifiable DNA from the Gypsum Cave coprolites (*6*). Therefore, to investigate the general state of macromolecular preservation in the coprolites, we performed chemical analyses.

Several samples were removed from a large fecal bolus. One was dated by accelerator mass spectrometry to 19,875 ± 215 years (Ua11835). Another sample was subjected to pyrolysis gas chromatography–mass spectrometry (Py-GC-MS). The pyrolysate (Fig. 1A) was dominated by products related to polysaccharides (cellulose and hemicellulose) and lignin. Minor pyrolysis products derived from proteins were also observed. Although some oxidation of lignin is evident, the relative abundance of polysaccharide products, and especially the hemicellulose derivative, suggest a relatively high degree of chemical preservation of ligno-cellulose (*7*). The large amount of syringol derivatives demonstrates that angiosperm lignin dominates in the coprolite, whereas the presence of vinylphenol can be attributed to monocotyledonous lignin.

The volatile components of another sample of the bolus were analyzed by head space GC-MS (*8*) (Fig. 1B). Alkylpyrazines, furanones, and furaldehydes, all products of the condensation of carbonyl groups of reducing sugars with primary amines (the Maillard reaction) (*9*) were detected. Specifically, the alkylpyrazines are formed through condensation of dicarbonyl compounds with amino acids (*9, 10*), and the furan products are indicative of advanced stages of the Maillard reaction, which may result in extensive cross-linking of macromolecules (*9*) such as proteins (*11*) and nucleic acids (*12*). Maillard Products have been suggested to be a prominent component in ancient DNA extracts (*13*) and were recently found in ancient Egyptian plant remains (*8*).

Because these analyses indicated the presence of Maillard products, *N*-phenacylthiazolium bromide (PTB), a reagent that cleaves glucose-derived protein cross-links (*14*), was added to the extraction mixtures to release DNA that might be trapped within sugar-derived condensation products. Extractions were done with and without the addition of PTB (*15*) and amplifications of a 153–base pair (bp) DNA segment of the mitochondrial 12*S* ribosomal RNA (rRNA) gene were attempted (*16*). From all extracts with added PTB, PCR prod-

H. N. Poinar, M. Hofreiter, S. Pääbo, Max-Planck-Institute for Evolutionary Anthropology and Zoological Institute, University of Munich, Luisenstrasse 14, D-80333 Munich, Germany. W. G. Spaulding, Dames & Moore, 7115 Amigo Street, Suite 110, Las Vegas, NV 89119, USA. P. S. Martin, Desert Laboratory, Department of Geosciences, University of Arizona, Tucson, AZ 85721, USA. B. A. Stankiewicz, H. Bland, R. P. Evershed, Biogeochemistry Research Center, Department of Geology, University of Bristol, Wills Memorial Building, Queen's Road, Bristol, BS81RJ, UK. G. Possnert, Ångström Laboratory, Division of Ion Physics, P.O. Box 534, S-75121 Uppsala, Sweden.

*Present address: Shell E & P Technology Company, 3737 Bellaire Boulevard, Houston, TX 77025, USA.